Nucleon-nucleon scattering in a time-dependent treatment

J. Holz and W. Glöckle
Institut für Theoretische Physik II, Ruhruniversität Bochum, D-4630 Bochum, Federal Republic of Germany
(Received 18 November 1987)

The time-dependent Schrödinger equation is solved for NN scattering in the case of a one-boson-exchange potential. The method works in momentum space with a complex contour to damp the oscillations which build up for large times. Since we abandon a partial wave decomposition, the treatment is well suited for high energies. The behavior of various observables is displayed as a function of time. As a side effect, we gain some quantitative insight into how the stationary scattering process is approached.

I. INTRODUCTION

Scattering processes are usually treated in a stationary manner. The energy spreads of realistic wave packets are much smaller than energy intervals on which scattering amplitudes vary noticeably. This is of course the very reason that initial momentum distributions of beam particles drop out of scattering observables and therefore a stationary treatment is justified. Also from a practical point of view the solution of a Lippman-Schwinger equation for a two-nucleon t matrix, though containing a Cauchy singularity in momentum space, can rather easily be achieved. However, already for three particles this is no longer the case. The treatment of the free propagator singularity requires painful work to handle it properly. Therefore a glance at a time-dependent treatment of the scattering process, where obviously no singularities are present, is natural. Moreover, one may be curious to know how the initial momentum distribution, in a two-nucleon system for instance, changes in the course of the reaction time to the final one, or how the final polarization of a nucleon builds up in the course of time from an initially unpolarized situation. There are many articles[1] on time-dependent scattering processes in atomic and molecular physics, which all treat the problem in configuration space. In nuclear physics the forces mediated by meson exchanges are naturally given in momentum space. Also the time dependence of the momentum-space wave function shows up in the explicitly known phase factor $e^{-iE_q t}$, which is easier to control numerically than the strong variations of the configuration-space wave function for instance near the edges of the potential.[2] Therefore we performed this study for time-dependent NN scattering mediated by meson exchanges in momentum space. The search for simplicity was also the motivation to work directly with vectors thereby avoiding the tedious partial-wave decomposition of an one-boson exchange (OBE) potential. This leaves the potential in its simple analytical form. In a previous study[3] we formulated and solved time-dependent potential scattering in momentum space. An example presented there clearly demonstrates the advantage of working with vector variables directly in comparison to a partial-wave decomposition. We shall refer to that work as I. We rely on I in Sec. II, where we formulate the equations for time-dependent potential scattering including a contour deformation of momenta to damp the large time oscillations. The treatment of two spin-$\frac{1}{2}$ particles based only on vector variables is worked out in Sec. III. The numerical performance and its accuracy is described in Sec. IV. Our results and pictures for the time evolution of the NN-scattering process are shown in Sec. V. Section VI contains the summary. Finally the Appendixes contain for the convenience of the reader the expressions of the NN potential we use, some details arising from our treatment of two spin-$\frac{1}{2}$ particles, and a discussion of the overlap of a stationary scattering state with the initial wave packet for large negative times.

II. FORMALISM

It is well known that time-dependent scattering states $\psi(t)$ are uniquely related to time-dependent free states $\psi_0(t)$, which describe the situation before the particles can interact. This connection is expressed by

$$\psi(t)=\Omega^{(+)}\psi_0(t)\ , \tag{2.1}$$

where $\Omega^{(+)}$ is the Möller wave operator, given for potential scattering by

$$\Omega^{(+)}=s-\lim_{\tau\to-\infty} e^{i(H_0+V)\tau}e^{-iH_0\tau}\ . \tag{2.2}$$

H_0 is the operator of kinetic energy and V the interaction. This is equivalent to saying

$$\lim_{t\to-\infty}\|\psi(t)-\psi_0(t)\|=0\ . \tag{2.3}$$

Let

$$\Omega(t_0-t)\equiv e^{iH(t_0-t)}e^{-iH_0(t_0-t)}\ , \tag{2.4}$$

then

$$\begin{aligned}\psi_{t_0}(t)&\equiv\Omega(t_0-t)\psi_0(t)\\&=e^{iH(t_0-t)}e^{-iH_0(t_0-t)}\psi_0(t)\\&=e^{-iH(t-t_0)}\psi_0(t_0)\end{aligned} \tag{2.5}$$

is a solution of the time-dependent Schrödinger equation, which coincides with the wave packet $\psi_0(t)$ at $t=t_0$. Because of the existence of the strong limit (2.2),

$$\|\psi(t)-\psi_{t_0}(t)\|=\|[\Omega^{(+)}-\Omega(t_0-t)]\psi_0(t)\|\to 0 \text{ , for } t_0\to-\infty \text{ .} \quad (2.6)$$

As a consequence if we rewrite the time-dependent Schrödinger equation into the integral form

$$\psi_{t_0}(t)=\psi_0(t)+\frac{1}{i}\int_{t_0}^{t} dt' e^{-iH_0(t-t')}V\psi_{t_0}(t') \text{ ,} \quad (2.7)$$

then the unique solution to that equation tends strongly for $t_0\to-\infty$ towards the scattering solution $\psi(t)$ defined in (2.1). Also the scattering solution $\psi(t)$ obeys

$$\psi(t)=\psi_0(t)+\frac{1}{i}\int_{-\infty}^{t} dt' e^{-iH_0(t-t')}V\psi(t') \text{ .} \quad (2.8)$$

In an actual calculation, as we are going to present, one has to live with a finite t_0, and one determines the state $\psi_{t_0}(t)$. The error induced can be discussed in the following manner. We expand the time development operator in (2.5) into the complete set of stationary scattering states $|\mathbf{q}\rangle^{(+)}$ and possible bound states $|n\rangle$:

$$\psi_{t_0}(t)=\int d^3q\ |\mathbf{q}\rangle^{(+)} e^{-iE_q(t-t_0)}{}^{(+)}\langle\mathbf{q}\,|\,\psi_0(t_0)\rangle + \sum_n |n\rangle e^{-iE_n(t-t_0)}\langle n\,|\,\psi_0(t_0)\rangle \text{ ,} \quad (2.9)$$

where the E_n are the bound-state energies and $E_q=q^2/m$ with m the nucleon mass. Clearly for any finite t_0, bound states overlap at least with the tails of the initial wave packet $\psi_0(t_0)$ and the solution $\psi_{t_0}(t)$ of Eq. (2.7) has bound states mixed in. Their strength, though, can be made arbitrarily small with decreasing t_0 as is obvious from applying the Riemann-Lebesgue lemma to $\langle n\,|\,\psi_0(t_0)\rangle$. The more delicate discussion of the amplitude ${}^{(+)}\langle\mathbf{q}\,|\,\psi_0(t_0\rangle$ is deferred to Appendix A. It is shown that for $t_0\to-\infty$ that amplitude reduces to the expected form $\langle\mathbf{q}\,|\,\psi_0(t_0)\rangle$. Thus for $t_0\to-\infty$ it gives

$$\psi(t)=\int d^3q\ |\mathbf{q}\rangle^{(+)} e^{-iE_q t}\psi_0(\mathbf{q}) \text{ ,} \quad (2.10)$$

where $\psi_0(\mathbf{q})$ describes the initial momentum distribution:

$$\langle\mathbf{q}\,|\,\psi_0(t)\rangle\equiv e^{-iE_q t}\psi_0(\mathbf{q})\equiv\psi_0(\mathbf{q},t) \text{ .} \quad (2.11)$$

In the following analytical considerations we work with expressions where the limit $t_0\to-\infty$ has been performed. As is easily derived from (2.8) and (2.10) and shown in I the scattering state in the momentum representation

$$\psi(\mathbf{q},t)\equiv\langle\mathbf{q}\,|\,\psi(t)\rangle \quad (2.12)$$

behaves asymptotically for $t\to\infty$ as

$$\psi(\mathbf{q},t)\to e^{-iE_q t}\left[\psi_0(\mathbf{q})-2\pi i\int d^3q' T(\mathbf{q},\mathbf{q}')\delta(E_q-E_{q'})\times\psi_0(\mathbf{q}')\right] \text{ .} \quad (2.13)$$

The scattered part in (2.13) contains the on-shell T matrix for all energies fed into the scattering process by the initial momentum distribution $\psi_0(\mathbf{q})$ and averaged over the angular spread of ψ_0. Since ψ_0 is freely at our disposal in the calculation we can use a wave packet with zero angular spread. Then $\psi(\mathbf{q},t)$ delivers asymptotically exactly the quantity T needed to calculate the various conventional observables. The typical time factor, $e^{-iE_q t}$, in a momentum-space representation causes serious numerical problems for large $|t|$ values. For large negative times where one has only the free wave packet (2.11) this problem can be trivially avoided by regarding only the scattered part of the wave function:

$$R(\mathbf{q},t)\equiv\psi(\mathbf{q},t)-\psi_0(\mathbf{q},t) \text{ .} \quad (2.14)$$

For large positive times, however, the outgoing wave packet carrying that phase factor is not known. In I we introduced a method which propagates suitable wave packets from negative *and* positive times forward and backward towards $t=0$, thereby eliminating the oscillations. The second method we proposed in I, though, is the one we use in this study. It is based on (2.8) rewritten for R:

$$R(\mathbf{q},t)=R_0(\mathbf{q},t)+\frac{1}{i}\int_{-\infty}^{t} dt' e^{-iE_q(t-t')}\times\int d^3q' V(\mathbf{q},\mathbf{q}')R(\mathbf{q}',t') \text{ .} \quad (2.15)$$

Thereby the scattered part in first order in V is

$$R_0(\mathbf{q},t)=\frac{1}{i}\int_{-\infty}^{t} dt' e^{-iE_q(t-t')}\int d^3q' V(\mathbf{q},\mathbf{q}')\psi_0(\mathbf{q}',t') \text{ .} \quad (2.16)$$

The problem with (2.15) lies in the limit of large positive t values, which are necessary to extract T and where one encounters the oscillations. If we could choose complex momenta $|\mathbf{q}|=le^{-i\pi/4}$, $l>0$, we could remove the oscillating phase factor in the kernel. However, an analytical continuation of (2.15) in the magnitude of $\mathbf{q}$ may hit potential singularities (we do not want to replace the propagator singularity in a time-independent treatment by potential singularities in a time-dependent treatment). For NN scattering, meson theoretical potentials contain meson propagators (or denominators of form factors) of the type $[(\mathbf{q}-\mathbf{q}')^2+\mu^2]^{-1}$, which can acquire a singularity for q complex and q' real. In the driving term (2.16) we are forced to keep the momenta q' real in order to avoid an exponential increase for negative times. The problem is solved in the following manner. We choose $\psi_0(\mathbf{q})$ such that it is strictly zero outside a certain momentum interval, say $[q_0-\Delta,q_0+\Delta]$, where q_0 is the central momentum in the beam. Then it is easily seen and shown in I that momenta $|\mathbf{q}|=l(1-i\alpha)$, $l>0$, avoid singularities of the meson propagators provided $0<\alpha<\mu/(q_0+\Delta)$. This restriction in α guarantees[4] at the same time the analytical continuation of Eq. (2.15) to complex momenta $|\mathbf{q}|=l(1-i\alpha)$, $l>0$, and $|\mathbf{q}'|=l'(1-i\alpha)$, $l'>0$. This form of Eq. (2.15) for momenta along the complex straight line $l(1-i\alpha)$, $l>0$, is used in our study. As the actual calculations show, the complex momenta strongly damp the oscillations, whereas a performance on the real axis leads to an uncontrolled behavior of R (see Sec. IV). Once R is determined

for complex momenta, Eq. (2.15) is used again as an integral representation for $R(\mathbf{q},t)$ evaluated at real momenta $\mathbf{q}$. Taking sufficiently large t values, the on-shell T matrix can be read off.

Equation (2.15) is an integral equation in the vector variable $\mathbf{q}$ and the time t. For NN scattering, R itself is a four component column vector. Clearly a reduction of variables is welcome. We achieve this in the following manner. In the Schrödinger picture the time evolution is propagated by $e^{-iH_0(t-t')}$ as explicitly seen in the kernels of (2.8) or (2.15). We split the total time elapsed, $T=2\,|\,t_0\,|$, into equally spaced intervals of length ΔT. Within the kth interval Eq. (2.15) reads, back in operator notation,

$$R(t)=R^{(t_k)}(t)+\frac{1}{i}\int_{t_k}^{t}dt'e^{-iH_0(t-t')}VR(t')\ , \tag{2.17}$$

where $R^{(t_k)}(t)$ is known from the previous interval. Since the time evolution operator in the Schrödinger picture depends only on $t-t'$, the integral in (2.17) can obviously be rewritten as

$$\int_{t_k}^{t}dt'e^{-iH_0(t-t')}VR(t')=\int_{0}^{\tau}d\tau'e^{-iH_0(\tau-\tau')}\times VR(\tau'+t_k)\ , \tag{2.18}$$

showing that the kernel acting on R is independent of k. In addition, if we choose small enough intervals, $R(t)$ can be interpolated linearily. Thus for the kth interval with $t_{k+1}=t_k+\Delta T$ we set

$$R(t)=R(t_k)\left[\frac{t_k+\Delta T-t}{\Delta T}\right]+R(t_{k+1})\left[\frac{t-t_k}{\Delta T}\right]\ . \tag{2.19}$$

Then the time integral in (2.17) can be performed analytically and we end up with

$$\begin{aligned}R(\mathbf{q},t_{k+1})=&R^{(t_k)}(\mathbf{q},t_{k+1})\\&+\frac{1}{i}K_{21}(\mathbf{q},\Delta T)\int d^3q'V(\mathbf{q},\mathbf{q}')R(\mathbf{q}',t_k)\\&+\frac{1}{i}K_{22}(\mathbf{q},\Delta T)\int d^3q'V(\mathbf{q},\mathbf{q}')R(\mathbf{q}',t_{k+1})\ .\end{aligned} \tag{2.20}$$

The simple analytical expressions K result from the explicit time integration and are given in I together with higher-order interpolating schemes replacing (2.19). Equation (2.20) allows us to calculate $R(t_{k+1})$ from $R(t_k)$, and what is the decisive point, with the help of an integral kernel which is independent of k. Therefore the inversion involved has to be performed only once.

We end this section with a remark on calculating bound states. One can maximize the admixture of bound states in $\psi_{t_0}(t)$ by choosing $t_0=0$. Then one starts the time propagation with a free wave packet located in the middle of the potential. For the sake of simplicity let us assume that V supports just one bound state. Then (2.9) tells us that $\psi_{t_0=0}(\mathbf{q},t)$ behaves for $t\to\infty$ as

$$\psi_{t_0=0}(t)\to e^{-iE_qt}C(\mathbf{q})+\varphi_n(\mathbf{q})e^{-iE_nt}C_n\ . \tag{2.21}$$

Choosing different times one can easily extract E_n and $\varphi_n(\mathbf{q})$.

III. APPLICATION TO NN SCATTERING

NN scattering can be successfully described by meson exchanges and even by an OBE parametrization thereof. A recent version[5] of the one-boson exchange potential (OBEP) used in our study is given in Appendix B. These simple analytical expressions include all possible invariants formed out of the initial and final relative momenta $\mathbf{q}$ and $\mathbf{q}'$ and the spin vectors $\boldsymbol{\sigma}_1$ and $\boldsymbol{\sigma}_2$. Invaince under rotation and parity transformation, and assuming isospin invariance, leads to the following general form for an interaction between two spin-$\frac{1}{2}$ particles

$$\begin{aligned}\mathbf{V}(\mathbf{q},\mathbf{q}')=&V_0+i(\boldsymbol{\sigma}_1+\boldsymbol{\sigma}_2)\cdot\mathbf{n}V_1+(\boldsymbol{\sigma}_1\cdot\mathbf{k})(\boldsymbol{\sigma}_2\cdot\mathbf{k})V_2\\&+(\boldsymbol{\sigma}_1\cdot\mathbf{p})(\boldsymbol{\sigma}_2\cdot\mathbf{p})V_3+(\boldsymbol{\sigma}_1\cdot\mathbf{n})(\boldsymbol{\sigma}_2\cdot\mathbf{n})V_4\\&+[(\boldsymbol{\sigma}_1\cdot\mathbf{k})(\boldsymbol{\sigma}_2\cdot\mathbf{p})+(\boldsymbol{\sigma}_1\cdot\mathbf{p})(\boldsymbol{\sigma}_2\cdot\mathbf{k})]V_5\ .\end{aligned} \tag{3.1}$$

We used $\mathbf{k}=\mathbf{q}-\mathbf{q}'$, $\mathbf{p}=\frac{1}{2}(\mathbf{q}+\mathbf{q}')$, and $\mathbf{n}=\mathbf{k}\times\mathbf{p}=\mathbf{q}\times\mathbf{q}'$. The functions V_i, $i=0,\ldots5$, depend only on q^2, q'^2, and $\mathbf{q}\cdot\mathbf{q}'$, and, because of time reversal invariance, V_5 is proportional to $\frac{1}{2}(q^2-q'^2)$. This factor vanishes on shell and reduces the six terms to the standard five expressions which occur in the analogous Wolfenstein parametrization of the NN-transition amplitude.[6] In the forms of the OBEP given in Appendix B three of the terms in Eq. (3.1) are hidden in $\boldsymbol{\sigma}_1\cdot\boldsymbol{\sigma}_2$, which can be expressed as

$$(\mathbf{k}\times\mathbf{p})^2\boldsymbol{\sigma}_1\cdot\boldsymbol{\sigma}_2=\mathbf{p}^2(\boldsymbol{\sigma}_1\cdot\mathbf{k})(\boldsymbol{\sigma}_2\cdot\mathbf{k})+\mathbf{k}^2(\boldsymbol{\sigma}_1\cdot\mathbf{p})(\boldsymbol{\sigma}_2\cdot\mathbf{p})+(\boldsymbol{\sigma}_1\cdot\mathbf{n})(\boldsymbol{\sigma}_2\cdot\mathbf{n})-(\mathbf{k}\cdot\mathbf{p})^2[(\boldsymbol{\sigma}_1\cdot\mathbf{k})(\boldsymbol{\sigma}_2\cdot\mathbf{p})+(\boldsymbol{\sigma}_1\cdot\mathbf{p})(\boldsymbol{\sigma}_2\cdot\mathbf{k})]\ . \tag{3.2}$$

Can the decomposition (3.1) of $\mathbf{V}$ be carried over to the scattering state $\psi(t)$? The initial state $\psi_0(t)$ is a four-component spinor according to the four possible initial spin orientations

$$\begin{bmatrix}1\\0\\0\\0\end{bmatrix},\ \begin{bmatrix}0\\1\\0\\0\end{bmatrix},\ \begin{bmatrix}0\\0\\1\\0\end{bmatrix},\ \begin{bmatrix}0\\0\\0\\1\end{bmatrix}\ . \tag{3.3}$$

To each choice of the initial spinor corresponds a spinor $\psi(t)$. The four possibilities can be combined into 4×4 matrices $\boldsymbol{\psi}_0(t)$ and $\boldsymbol{\psi}(t)$, which obey

$$\boldsymbol{\psi}(t)=\boldsymbol{\psi}_0(t)+\frac{1}{i}\int_{-\infty}^{t}dt'e^{-iH_0(t-t')}\mathbf{V}\boldsymbol{\psi}(t')\ , \tag{3.4}$$

where

$$\psi_0(t)=\psi_0(t)\begin{bmatrix}1&0&0&0\\0&1&0&0\\0&0&1&0\\0&0&0&1\end{bmatrix}. \tag{3.5}$$

One can study[4] the invariance properties of Eq. (3.4) under rotation and parity transformations. We use an initial momentum distribution $\psi_0(\mathbf{q})$ which is centered around a mean momentum $\mathbf{q}_0$ and is a scalar function $\psi_0((\mathbf{q}-\mathbf{q}_0)^2)$ [see Eq. (4.1) for the form we use]. The result is that $\psi(t)$ behaves like $\mathbf{V}$ and can therefore be decomposed analogous to (3.1). The same conclusion is reached by regarding the perturbation series of (3.4). Therefore the decomposition for ψ and consequently for the scattered part $\mathbf{R}$ we use in the actual calculation, reads

$$\begin{aligned}\mathbf{R}(\mathbf{q},t)=&R_0+i(\sigma_1+\sigma_2)\cdot\mathbf{n}_0R_1+(\sigma_1\cdot\hat{\mathbf{k}}_0)(\sigma_2\cdot\hat{\mathbf{k}}_0)R_2+(\sigma_1\cdot\hat{\mathbf{p}}_0)(\sigma_2\cdot\hat{\mathbf{p}}_0)R_3\\&+(\sigma_1\cdot\hat{\mathbf{n}}_0)(\sigma_2\cdot\hat{\mathbf{n}}_0)R_4+((\sigma_1\cdot\hat{\mathbf{k}}_0)(\sigma_2\cdot\hat{\mathbf{p}}_0)+(\sigma_1\cdot\hat{\mathbf{p}}_0)(\sigma_2\cdot\hat{\mathbf{k}}_0))R_5\,,\end{aligned} \tag{3.6}$$

where $\hat{\mathbf{n}}_0$, $\hat{\mathbf{k}}_0$, and $\hat{\mathbf{p}}_0$ depend on $\mathbf{q}$ and $\mathbf{q}_0$. Since the momenta $\mathbf{q}$ are, in general, off-shell it is convenient to introduce the orthonormal basis vectors

$$\hat{\mathbf{k}}_0=\frac{\hat{\mathbf{q}}-\hat{\mathbf{q}}_0}{|\hat{\mathbf{q}}-\hat{\mathbf{q}}_0|}\,, \tag{3.7}$$

$$\hat{\mathbf{p}}_0=\frac{\hat{\mathbf{q}}+\hat{\mathbf{q}}_0}{|\hat{\mathbf{q}}+\hat{\mathbf{q}}_0|}\,, \tag{3.8}$$

$$\hat{\mathbf{n}}_0=\hat{\mathbf{k}}_0\times\hat{\mathbf{p}}_0=\frac{\hat{\mathbf{q}}\times\hat{\mathbf{q}}_0}{|\hat{\mathbf{q}}\times\hat{\mathbf{q}}_0|} \tag{3.9}$$

in order to keep the various terms in (3.6) orthogonal to each other with respect to taking the trace. Now a straightforward procedure would be to insert the decompositions (3.1) and (3.6) into the integral equation for $\mathbf{R}(\mathbf{q},t)$, which is the analogue of (2.15) in the spin-dependent case, and project by appropriate traces onto the individual R_i's. It would give six coupled equations for the scalar functions R_i. Fortunately there is a much simpler way. $\psi(t)$ is a 4×4 matrix built up by six independent scalar functions. How are they distributed over the 16 positions? We choose a fixed coordinate system such that

$$\hat{\mathbf{q}}_0=\begin{bmatrix}0\\0\\1\end{bmatrix},\qquad \hat{\mathbf{q}}=\begin{bmatrix}\sin\theta\\0\\\cos\theta\end{bmatrix},\qquad \hat{\mathbf{q}}'=\begin{bmatrix}\sin\theta'\cos\varphi'\\\sin\theta'\sin\varphi'\\\cos\theta'\end{bmatrix}. \tag{3.10}$$

Then the orthonormal basis vectors (3.7)–(3.9) turn out to be ($z'=\hat{\mathbf{q}}'\cdot\hat{\mathbf{q}}_0$)

$$\hat{\mathbf{k}}_0'=\frac{1}{\sqrt{2}}\begin{bmatrix}\sqrt{1+z'}\cos\varphi'\\\sqrt{1+z'}\sin\varphi'\\-\sqrt{1-z'}\end{bmatrix},\qquad \hat{\mathbf{p}}_0'=\frac{1}{\sqrt{2}}\begin{bmatrix}\sqrt{1-z'}\cos\varphi'\\\sqrt{1-z'}\sin\varphi'\\\sqrt{1+z'}\end{bmatrix}, \tag{3.11}$$

$$\hat{\mathbf{n}}_0'=\begin{bmatrix}\sin\varphi'\\-\cos\varphi'\\0\end{bmatrix},$$

which include the special case $\hat{\mathbf{k}}_0$, $\hat{\mathbf{p}}_0$, $\hat{\mathbf{n}}_0$ for $\varphi'=0$ and $z'=z=\hat{\mathbf{q}}\cdot\hat{\mathbf{q}}_0$. Inserting then the Pauli matrices explicitly into (3.6) leads to $\mathbf{R}(\mathbf{q}',t')$ in the $|m_1m_2\rangle$ representation:

$$\mathbf{R}(\mathbf{q}',t')=\begin{bmatrix}S_1&S_4e^{-i\varphi'}&S_4e^{-i\varphi'}&S_3e^{-2i\varphi'}\\S_2e^{i\varphi'}&S_5&S_6&-S_2e^{-i\varphi'}\\S_2e^{i\varphi'}&S_6&S_5&-S_2e^{-i\varphi'}\\S_3e^{2i\varphi'}&-S_4e^{i\varphi'}&-S_4e^{i\varphi'}&S_1\end{bmatrix} \tag{3.12}$$

with ($z'=\hat{\mathbf{q}}'\cdot\hat{\mathbf{q}}_0$)

$$\begin{aligned}S_1&=R_0+\tfrac{1}{2}(1-z')R_2+\tfrac{1}{2}(1+z')R_3-\sqrt{1-z'^2}R_5\,,\\S_2&=R_1-\tfrac{1}{2}\sqrt{1-z'^2}(R_2-R_3)+z'R_5\,,\\S_3&=\tfrac{1}{2}(1+z')R_2+\tfrac{1}{2}(1-z')R_3-R_4+\sqrt{1-z'^2}R_5\,,\end{aligned} \tag{3.13}$$

$$\begin{aligned}S_4&=-R_1-\tfrac{1}{2}\sqrt{1-z'^2}(R_2-R_3)+z'R_5\,,\\S_5&=R_0-\tfrac{1}{2}(1-z')R_2-\tfrac{1}{2}(1+z')R_3+\sqrt{1-z'^2}R_5\,,\\S_6&=\tfrac{1}{2}(1+z')R_2+\tfrac{1}{2}(1-z')R_3+R_4+\sqrt{1-z'^2}R_5\,.\end{aligned}$$

One discovers six linear combinations S_i which are distributed over the 4×4 matrix such that in each column there occurs just three of them. Consequently (3.4) has to decay into two sets of three coupled equations (corresponding to the first two columns). In order to achieve these sets one has to work out the 4×4 matrix representation of $\mathbf{V}$, Eq. (3.1). This is straightforward and the result is displayed in Appendix C. The remaining matrix multiplication of $\mathbf{V}$ and $\mathbf{R}$ in the integral term of Eq. (2.4) is easily performed and it gives the two sets of coupled equations,

$$S_i(q,z,t)=S_i^{(0)}(q,z,t)+\frac{1}{i}\int_{-\infty}^{t}dt' e^{-iE_q(t-t')}\sum_{\alpha=0}^{5}\int_0^\infty dq' q'^2\int_{-1}^{1}dz'\int_0^{2\pi}d\varphi' V_\alpha(q,q',y)J_i^{(\alpha)} \times(q,z,q',z',\varphi',t') , \tag{3.14}$$

for $i=1,2,3$ and $i=4,5,6$, respectively. The terms $J_i^{(\alpha)}$ are linear combinations of the S_i's and are displayed in Appendix C. We recognize that the dependence on the vector variable $\mathbf{q}$ shows up as a dependence on $q=|\mathbf{q}|$ and $z=\hat{\mathbf{q}}\cdot\hat{\mathbf{q}}_0$. The azymuthal angle φ' occurs in the variable

$$y=\hat{\mathbf{q}}\cdot\hat{\mathbf{q}}'=zz'+\sqrt{1-z^2}\sqrt{1-z'^2}\cos\varphi' \tag{3.15}$$

and as factors $\cos\varphi'$ and $\sin\varphi'$ within $J_i^{(\alpha)}$. Though the φ' integral can be performed analytically, it is more transparent in the actual calculation to do it numerically. The time integrations in the two sets (3.14) are handled as described in Sec. II leading to the structure (2.20). Then the equations are solved by rotating the momenta into the complex plane. For large times t the asymptotic on-shell values S_i are extracted and rewritten via (3.13) into the amplitudes R_i for the scattered part $\mathbf{R}$ in Eq. (3.6). Then in a standard manner the observables are determined as we describe in Sec. V. We would like to emphasize that this method determines the on-shell T matrix for NN scattering directly without partial-wave decomposition and scattering phase-shift parameters.

IV. NUMERICAL PERFORMANCE

We choose the wave packets in the form

$$\psi_0(\mathbf{q})=\delta(\hat{\mathbf{q}}-\hat{\mathbf{q}}_0)f_0(q)=\delta(\hat{\mathbf{q}}-\hat{\mathbf{q}}_0)\begin{cases}\left[\frac{\sigma}{\sqrt{\pi}}\right]^{3/2}e^{-(\sigma^2/2)(q-q_0)^2}, & \text{for } q_0-\Delta\le q\le q_0+\Delta ,\\ 0, & \text{otherwise .}\end{cases} \tag{4.1}$$

Their parameters are given in Table I. We use $m=4.758$ fm. The minimum and maximum energies related to $q_0-\Delta$ and $q_0+\Delta$ are denoted by $E_{\min}$ and $E_{\max}$. The q' and z' integrations are performed by Gaussian quadrature with typically 35 and 13 points, respectively. This refers to wave packets Nos. 1–3, whereas the number of quadrature points could even be reduced for wave packet No. 4. This is sufficient to achieve an accuracy of three digits in the on-shell T matrices. It is important to locate most of the q points between 0 and $q_0+\Delta$. The remaining ones are distributed between $q_0+\Delta$ and a numerically determined cutoff value around 50 fm^{-1}. In case of strong forward scattering induced by wave packet No. 2 (see Sec. V) the values $z'>0$ should be more heavily populated than $z'<0$ whereas for the other cases we distributed the z' values symmetrically around $z=0$. Table I also shows the angles α for the complex contours and the initial time t_0 together with the lengths ΔT of the small time intervals within which R is interpolated linearily. Wave packet No. 1 is used for NN scattering on a Malfliet-Tjon potential and on an OBE potential. They have different ranges, which is reflected in the different α's. The small value $\alpha=0.3$ is due to the pion mass. Numerical details concerning the potential scattering of a spinless particle at a Malfliet-Tjon potential has been discussed in I where all necessary parameters are given. As an additional insight we show in Table II how the scattered part R varies in time and specifically approaches its asymptotic value.

With the exception of the edges of the initial momentum distribution we recognize stability within three digits. For additional figures exhibiting the smooth behavior of R along the complex path in contrast to the oscillating behavior for real momenta we refer to Refs. 3 and 4. In Ref. 4 it is also demonstrated that a direct solution of the integral equation (2.20) for real momenta leads already for relatively small positive times to deviations from the correct behavior and appears to be unfeasible.

In the case of NN scattering at the OBEP (Ref. 5) given in Appendix B we used the wave packets Nos. 1, 3, and 4. Only for the purpose of demonstrating the numerical accuracy, we calculated the standard phase-shift parameters (Stapp parametrization) from the full on-shell T matrix extracted at large positive times. According to (2.13)

$$\mathbf{R}(\mathbf{q},t)\underset{t\to\infty}{\longrightarrow}-\pi i m q e^{-iE_q t}\mathbf{T}(\mathbf{q},q\hat{\mathbf{q}}_0)f_0(q) . \tag{4.2}$$

The T matrix is given in the $|m_1m_2\rangle$ representation. By simple linear combinations it can be converted into the $|Sm_S\rangle$-representation

$$T^S_{m_S'm_S}(q,z)=\langle Sm_S'|T(\mathbf{q},q\hat{\mathbf{q}}_0)|Sm_S\rangle , \tag{4.3}$$

where S is the total two-nucleon spin. Then the partial-wave projection to a state of total angular momentum j reads

$$T^j_{l'S,lS}(q,q)=4\pi^{3/2}\frac{\sqrt{2l+1}}{2j+1}i^{l'-l}\sum_{m_Sm_S'}C(l'Sj,m_S-m_S',m_S',m_S)C(lSj,0m_Sm_S) \times\int_{-1}^{1}dz Y_{l'}^{m_S'-m_S*}(\theta,\varphi=0)T^S_{m_S'm_S}(q,z) , \tag{4.4}$$

TABLE I. Parameters of the wave packets used. The parameter α determines the complex contour, and ΔT is the length of the subintervals in time.

No.	Eq_0 (MeV)	q_0 (fm^{-1})	σ (fm)	Δ (fm^{-1})	$E_{\min}$ (MeV)	$E_{\max}$ (MeV)	α	t_0 (fm)	ΔT (fm)
1	50	1.10	7.5	0.5	14.9	106.2	0.7 (0.3)	−100	0.5
2	508	3.50	5.0	1.2	219.4	961.1	0.3	−20	0.05
3	100	1.55	7.5	0.5	45.7	174.3	0.25	−100	0.3
4	50	1.10	75.0	0.1	41.5	59.7	0.3	−600	0.5

TABLE II. The magnitude of the scattered part of the wave function, $|R(\mathbf{q},t)|$, for $\cos\theta=0$, as a function of time. The stationary behavior near $t=100$ fm is clearly visible.

q (fm^{-1})	$t=-70$ fm	−50 fm	−20 fm	0 fm	20 fm	50 fm	70 fm	100 fm
0.49	2.24×10^{-4}	3.22×10^{-3}	7.22×10^{-2}	1.27×10^{-1}	5.47×10^{-1}	1.70×10^{-3}	1.89×10^{-4}	1.32×10^{-4}
0.69	1.91×10^{-4}	3.26×10^{-3}	8.47×10^{-2}	1.67×10^{-1}	7.09×10^{-2}	1.02×10^{-2}	1.18×10^{-2}	1.19×10^{-2}
0.85	1.48×10^{-4}	2.93×10^{-3}	9.56×10^{-2}	2.59×10^{-1}	2.34×10^{-1}	1.74×10^{-1}	1.73×10^{-1}	1.73×10^{-1}
1.10	7.97×10^{-5}	1.83×10^{-3}	7.38×10^{-2}	2.86×10^{-1}	4.69×10^{-1}	5.60×10^{-1}	5.60×10^{-1}	5.60×10^{-1}
1.20	6.02×10^{-5}	1.34×10^{-3}	5.17×10^{-2}	1.90×10^{-1}	2.94×10^{-1}	2.78×10^{-1}	2.77×10^{-1}	2.77×10^{-1}
1.39	3.56×10^{-5}	6.82×10^{-4}	2.08×10^{-2}	6.16×10^{-2}	5.16×10^{-2}	1.90×10^{-2}	1.82×10^{-2}	1.82×10^{-2}
1.55	3.34×10^{-5}	3.39×10^{-4}	8.26×10^{-2}	3.06×10^{-2}	2.01×10^{-2}	6.96×10^{-4}	1.08×10^{-3}	1.11×10^{-3}

TABLE III. NN phase-shift parameters projected out of the full T matrix gained in a time-dependent treatment in comparison to phase-shift parameters calculated in the conventional partial-wave projected stationary treatment.

E_{CM} (MeV)	Time dependent	Time independent	Time dependent	Time independent
	$^1S_0$		$^3P_0$	
25.0	41.443	41.438	14.445	14.442
50.0	27.370	27.371	13.092	13.096
71.0	18.577	18.575	9.233	9.240
105.0	7.286	7.296	2.080	2.097
162.5	−7.263	−7.256	−9.435	−9.436
	$^1P_1$		$^3S_1$	
25.0	−10.886	−10.881	62.322	62.325
50.0	−15.099	−15.097	42.297	42.303
71.0	−17.380	−17.381	31.160	31.167
105.0	−19.828	−19.828	17.796	17.776
162.5	−21.529	−21.688	1.550	1.470
	ϵ_1		ϵ_2	
25.0	1.119	1.127	−1.916	−1.914
50.0	0.484	0.476	−3.044	−3.044
71.0	0.051	0.052	−3.325	−3.325
105.0	−0.435	−0.420	−3.115	−3.114
162.5	−0.822	−0.843	−2.050	−2.065

and the connection to the unitary S matrix is

$$S^j_{l'S,lS}(q)=\delta_{l'l}-i\pi mqT^j_{l'S,lS}(q,q)\ . \tag{4.5}$$

We show in Table III several phase-shift parameters in comparison to values gained by the standard stationary treatment,[7] which works directly in a partial-wave basis. The agreement is better than one percent except for the parameter ϵ_1, which is a small quantity.

In the spin-dependent problem the typical CPU time for one wave packet and one isospin is 1000 sec on a Cyber 205. Note that such a run covers for instance energies between 20 and 100 MeV.

As a further numerical test for the quality of the method and as an unconventional method to determine bound state energies we followed the time development of a wave packet starting at $t=0$ in the middle of the potential. Based on Eq. (2.21) we extracted the binding energy of the Malfliet-Tjon potential from the formula

$$e^{-iE_n\delta}=\frac{e^{iE_q\delta}R(q,z,t_2)-R(q,z,t_1)}{e^{iE_q\delta}R(q,z,t_1)-R(q,z,t_3)} \tag{4.6}$$

with $\delta=t_2-t_1=-(t_3-t_1)$. We have chosen $t_1=295$ fm, $t_2=300$ fm, and $t_3=290$ fm. The right-hand side of (4.6) should be independent of q,z and should be of magnitude 1. Our results are shown in Table IV. Note that the values obtained for E_n are in good agreement with the correct one, $E_n=-0.0113$ fm$^{-1}=-2.23$ MeV.

V. PICTORIAL INSIGHT INTO THE NN SCATTERING PROCESS

Let us first regard the scattering on the Malfliet-Tjon potential. The magnitude of the scattered part of the wave function, $R(\mathbf{q},t)$, is shown in Fig. 1. At the scale of the figure the very beginning of the scattering process at $t=-99$ fm is not visible. Around $t=0$ roughly half of the heights of the final values are achieved. Then for $t>0$ the forward and backward scattering become more pronounced. At intermediate times the energy is not conserved. This is clearly visible in the fact that around $t=0$, $|R(\mathbf{q},t)|$ decreases much more slowly than for large positive times. The interval in q depicted is nearly $(q_0-\Delta,q_0+\Delta)$ and $R(\mathbf{q},t)$ supports at intermediate times virtual momenta far outside that interval. For $t=100$ fm the final shape is strongly dominated by the initial momentum distribution $f_0(q)$. Only after dividing by that factor one is left, according to Eq. (4.2), with the on-shell T matrix as a function of energy and scattering angle.

More dramatic is the scattering process at higher energies delivered by the wave packet No. 2 which is shown in Fig. 2. Here the forward scattering is much more pronounced. A partial-wave representation (which we did

TABLE IV. Test for Eq. (4.6). The bound-state energy E_n extracted for various q and z values and the magnitude of the right-hand side are shown.

q (fm)$^{-1}$	z	E_n	Magnitude
0.49	−1.0	−0.0111	1.0008
0.49	0.0	−0.0111	1.0008
0.49	1.0	−0.0111	1.0007
1.10	−1.0	−0.0111	1.0009
1.10	0.0	−0.0111	1.0008
1.10	1.0	−0.0112	1.0005
1.55	−1.0	−0.0110	1.0011
1.55	0.0	−0.0110	1.0008
1.55	1.0	−0.0116	1.0001

not use) would require many terms.

Knowing the scattered part of the wave function $\mathbf{R}(t)$ at all times we can now determine how spin variables develop in time. As an example, let us regard how the polarization of one particle arises out of an unpolarized state:

$$\mathbf{P}_0(\mathbf{q},t)\equiv\frac{\mathrm{Tr}(\mathbf{R}(\mathbf{q},t)\mathbf{R}^+(\mathbf{q},t)\sigma)}{\mathrm{Tr}(\mathbf{R}(\mathbf{q},t)\mathbf{R}^+(\mathbf{q},t))}\ . \tag{5.1}$$

Because of parity conservation $\mathbf{P}_0$ is always orthogonal to the scattering plane. This quantity is shown in Fig. 3. For $t=100$ fm one can read off both the angular distribu-

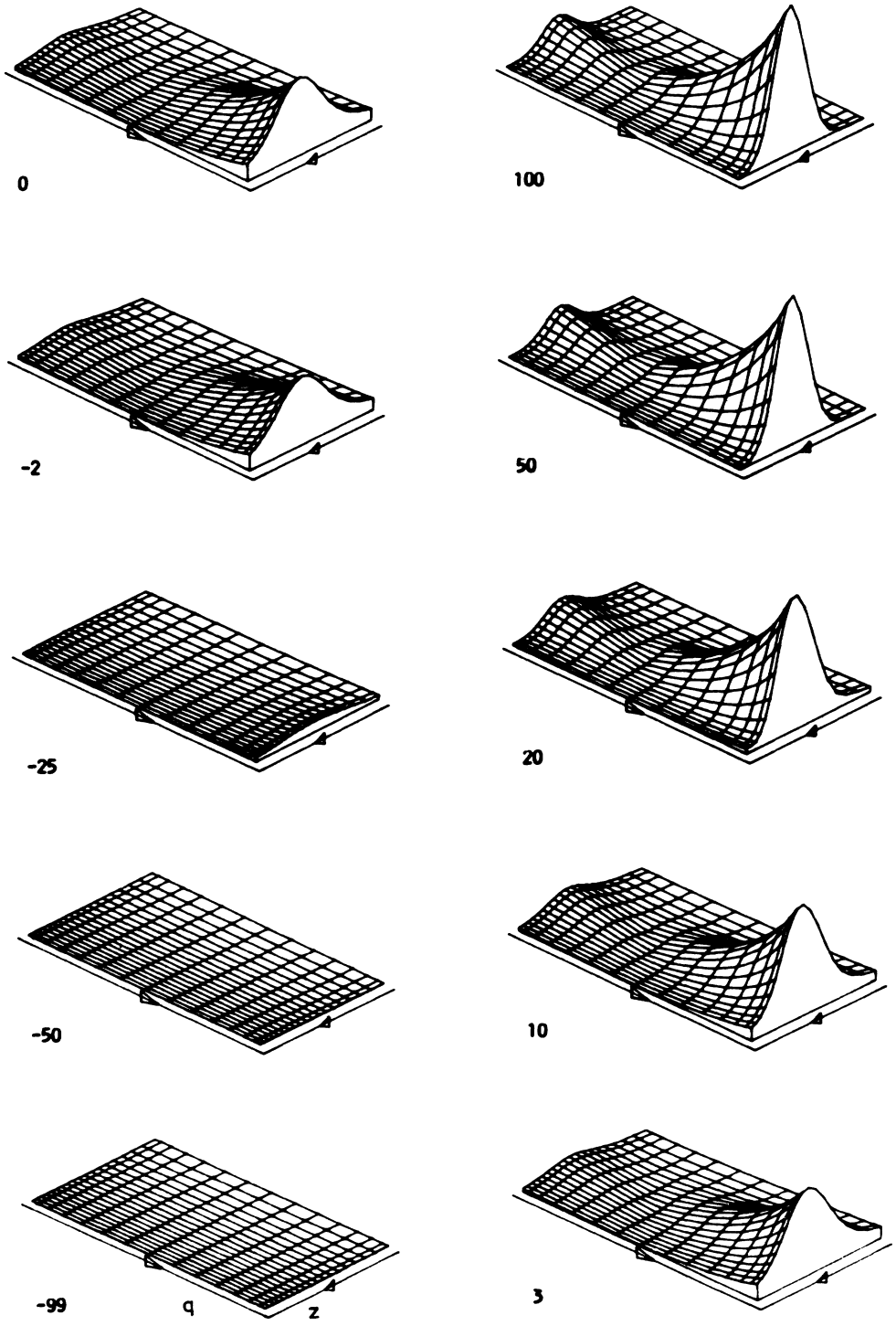

FIG. 1. The magnitude of the scattered part of the wave function $|R(q,z,t)|$ as a function of $z=\hat{\mathbf{q}}\cdot\hat{\mathbf{q}}_0$ and $q=|\mathbf{q}|$ for various times between $t=-99$ and 100 fm. This is for the Malfliet-Tjon potential and wave packet No. 1.

tion of P_0 for fixed energy and the energy variation of P_0 for fixed scattering angle. One recognizes strong qualitative deviations from the final values at positive and negative intermediate times. Inserting the formal solution for R derived from (2.10),

$$\mathbf{R}(\mathbf{q},t)=\int d^3q' e^{-iE_{q'}t}\psi_0(\mathbf{q}')\mathbf{T}(\mathbf{q},\mathbf{q}')\frac{1}{E_{q'}+i\epsilon-E_q}\ , \tag{5.2}$$

into (V.1), we get

$$P_0(\mathbf{q},t)=\left[\int d^3q'\frac{e^{-iE_{q'}t}\psi_0(\mathbf{q}')}{E_{q'}+i\epsilon-E_q}\int d^3q''\frac{e^{iE_{q''}t}\psi_0(\mathbf{q}'')}{E_q''-i\epsilon-E_q}\mathrm{Tr}(\mathbf{T}(\mathbf{q},\mathbf{q}')\mathbf{T}^+(\mathbf{q},\mathbf{q}'')\sigma)\right]$$
$$\times\left[\int d^3q'\frac{e^{-iE_{q'}t}\psi_0(\mathbf{q}')}{E_{q'}+i\epsilon-E_q}\int d^3q''\frac{e^{iE_{q''}t}\psi_0(\mathbf{q}'')}{E_{q''}-i\epsilon-E_q}\mathrm{Tr}(\mathbf{T}(\mathbf{q},\mathbf{q}')\mathbf{T}^+(\mathbf{q},\mathbf{q}''))\right]^{-1}. \tag{5.3}$$

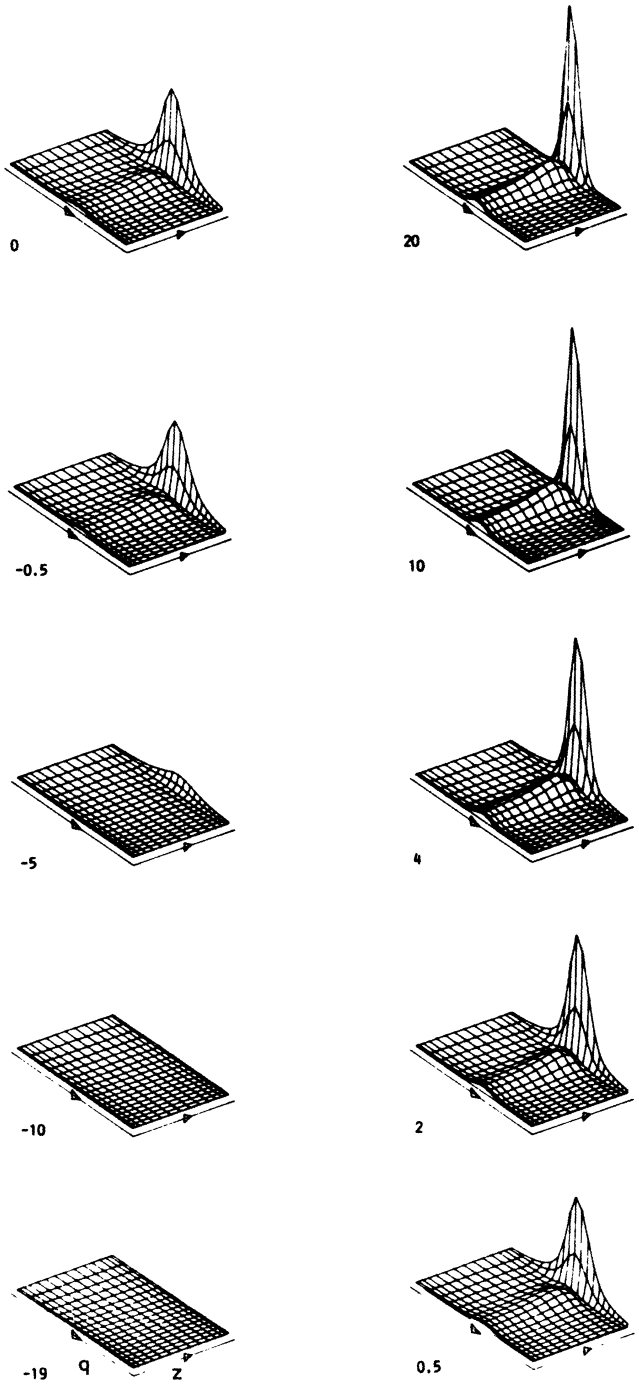

FIG. 2. The same as in Fig. 1 for wave packet No. 2.

This formula shows that the intermediate time structure in Fig. 3 results from an interplay of the shape of the initial wave packet, $\psi_0(\mathbf{q})$, and the half-shell properties of the NN T matrix $\mathbf{T}(\mathbf{q},\mathbf{q}')$.

The same quantity P_0 is shown in Fig. 4 for the wave packet No. 3, which is shifted to higher energies but has an overlap with energies contained in the wave packet No. 1 used to generate Fig. 3. Here the deviations at in-

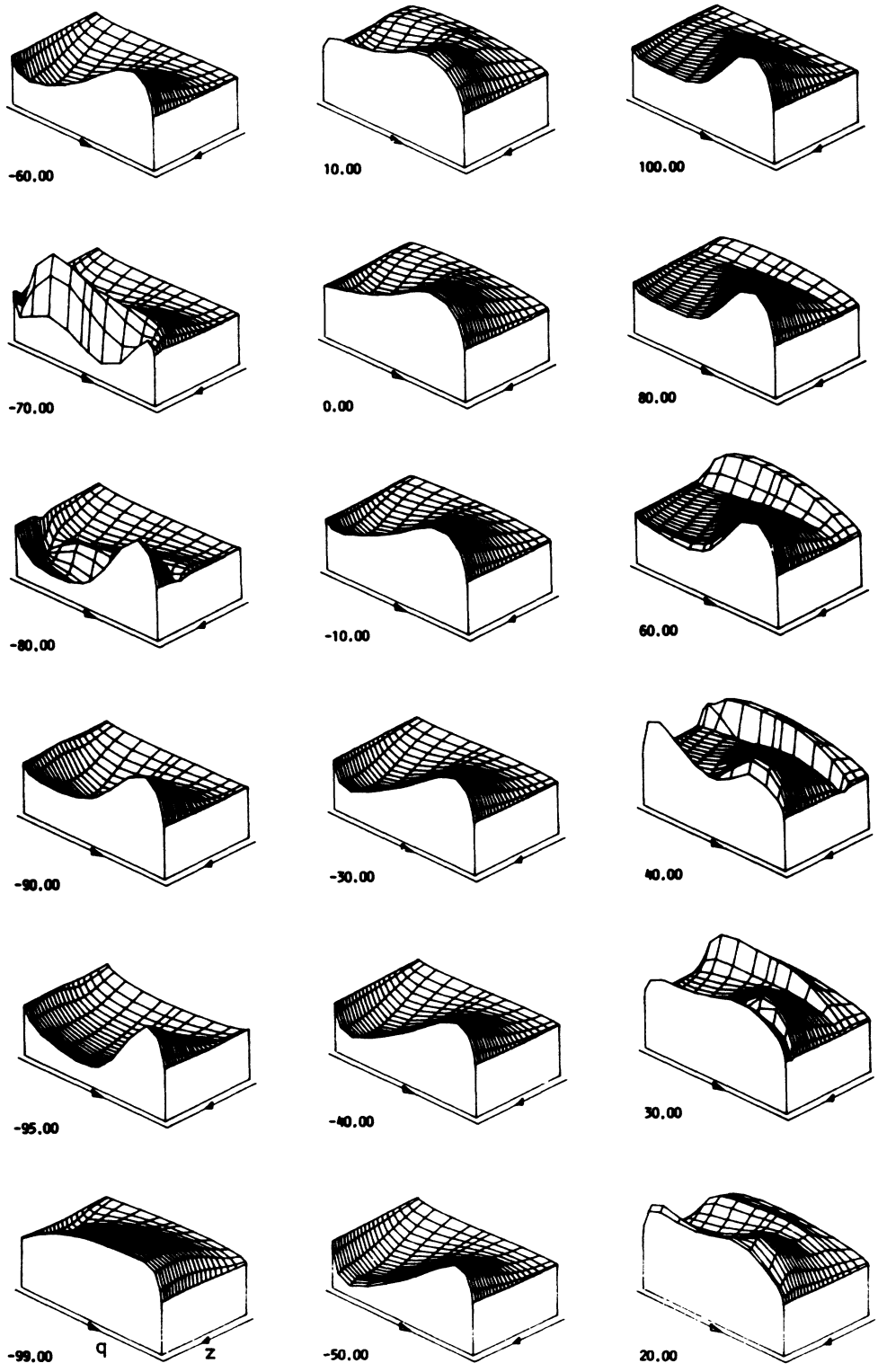

FIG. 3. The y component of $\mathbf{P}_0$ as a function of $z=\hat{\mathbf{q}}\cdot\hat{\mathbf{q}}_0$ and $q=|\mathbf{q}|$ for various times. This is for the OBE potential and wave packet No. 1. P_0 varies between -0.63 and 0.62.

termediate times from the final shape are different from the ones in Fig. 3. Of course, at sufficiently large positive times, here $t=100$ fm, where the dependence on the initial momentum distribution $f_0(q)$ drops out, the values agree in the overlap region. This can quantitatively be seen in Table V. As another example we choose an initial polarization $\mathbf{P}_i=\hat{\mathbf{e}}_y$ in the y direction. Note that the x and z directions span the scattering plane. The resulting polarization of one of the nucleons is

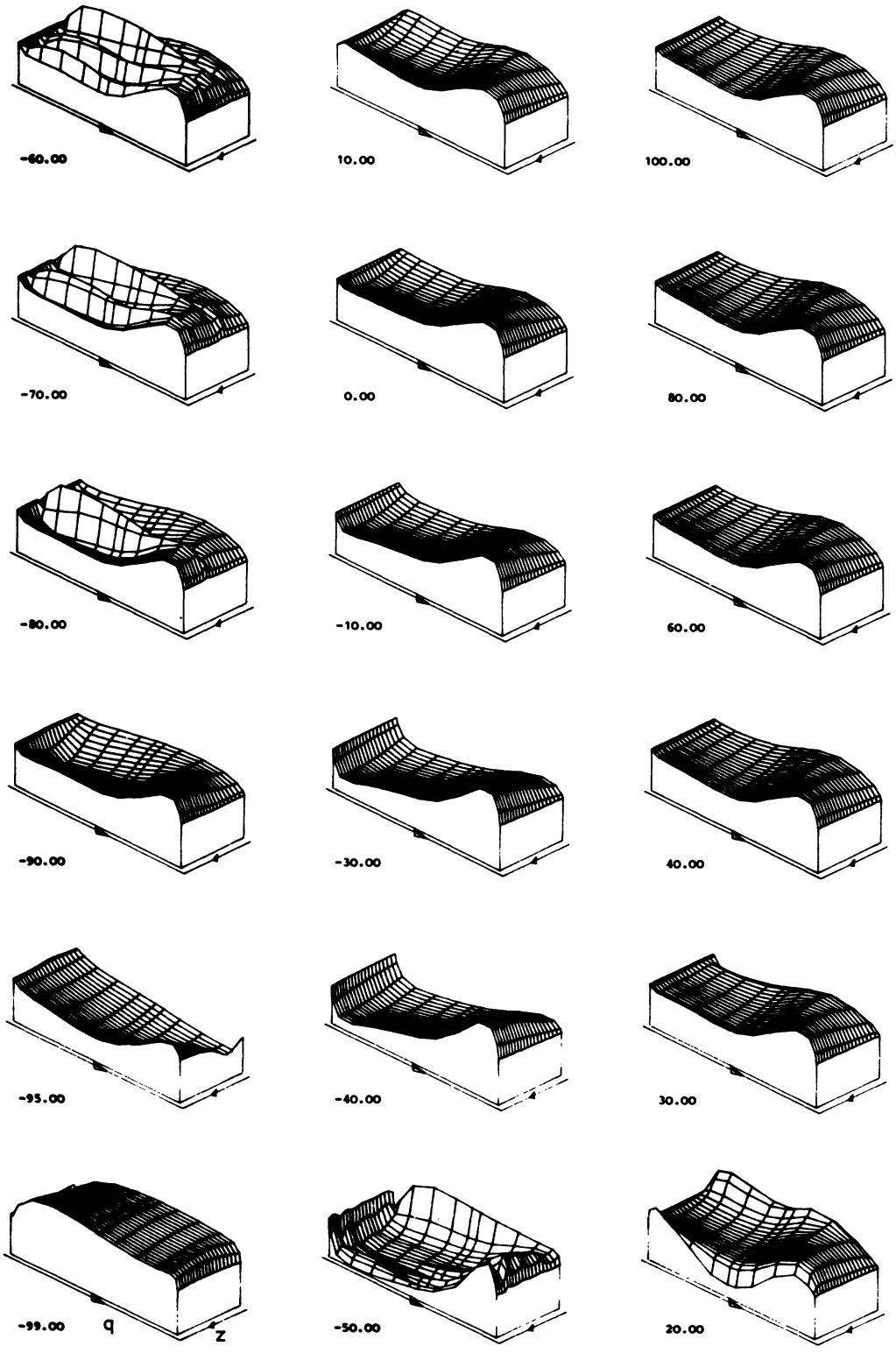

FIG. 4. The same as in Fig. 3 for wave packet No. 3. P_0 varies between -0.90 and 0.70.

$$\mathbf{P}(\mathbf{q},t)=[\mathrm{Tr}(\mathbf{R}(\mathbf{q},t)(1+\sigma\cdot\mathbf{P}_i)\mathbf{R}^{+}(\mathbf{q},t)\sigma)]\times[\mathrm{Tr}(\mathbf{R}(\mathbf{q},t)(1+\sigma\cdot\mathbf{P}_i)\mathbf{R}^{+}(\mathbf{q},t))]^{-1}\ . \quad (5.4)$$

The polarization in the y direction is shown in Fig. 5. The underlying wave packet is No. 3.

If the initial wave packets get sharper in energy, then one can take the T matrix out of the integral and the time dependence cancels between numerator and denominator

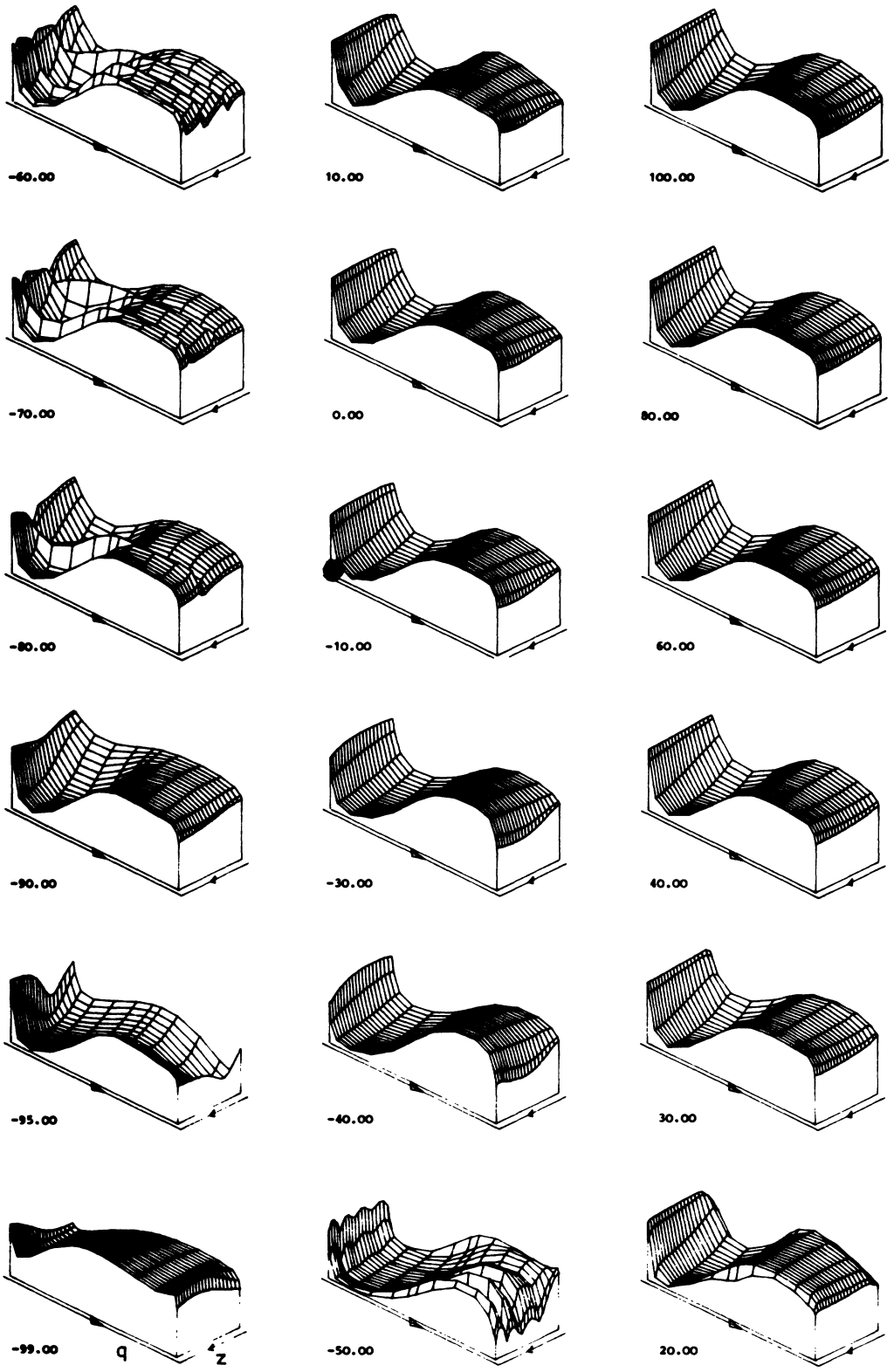

FIG. 5. The y component of $\mathbf{P}$ resulting from an initial polarization in y direction as a function of $z=\hat{\mathbf{q}}\cdot\hat{\mathbf{q}}_0$ and $q=|\mathbf{q}|$ for various times. This is for the OBE potential and wave packet No. 3. P_y varies between -0.97 and 1.00.

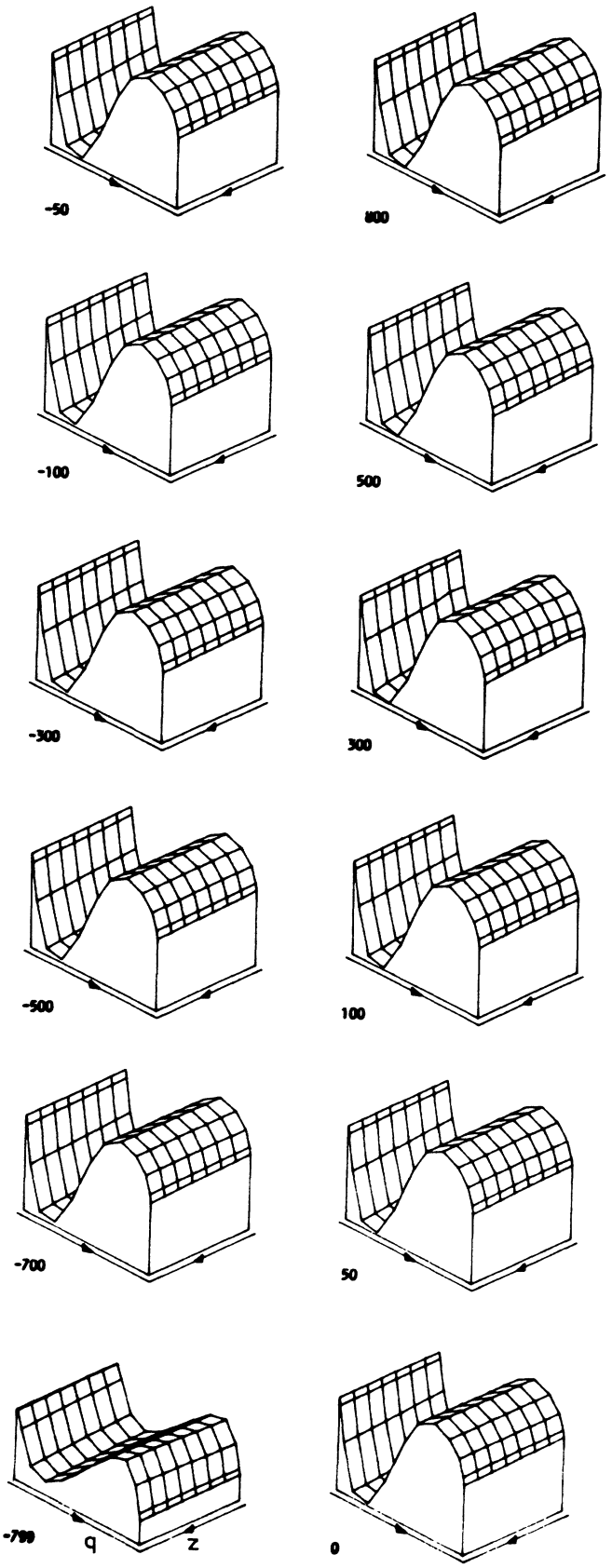

FIG. 6. The same as in Fig. 5 with wave packet No. 4. This is already sharp enough in energy to produce nearly stationary behavior. P_y varies between -0.14 and 1.00.

TABLE V. The y component of $\mathbf{P}_0$ for the two wave packets Nos. 1 and 3 which have an overlap for the momenta shown. The interference between the half-shell T matrix and the shape of the wave packet leads to different values during the collision time but to the same stationary values at large times.

q (fm^{-1})	z	No.	$t=-90$ fm	-50 fm	-10 fm	10 fm	50 fm	100 fm
1.15	−0.75	1	-3.10×10^{-1}	-3.00×10^{-1}	-2.12×10^{-1}	-1.65×10^{-1}	-1.37×10^{-1}	-1.38×10^{-1}
1.15	−0.75	3	-1.22×10^{-1}	-2.25×10^{-1}	-3.44×10^{-1}	-2.21×10^{-1}	-1.39×10^{-1}	-1.38×10^{-1}
1.39	0.51	1	2.21×10^{-1}	2.30×10^{-1}	1.48×10^{-1}	1.04×10^{-1}	1.69×10^{-1}	1.73×10^{-1}
1.39	0.51	3	2.69×10^{-1}	3.76×10^{-1}	2.54×10^{-1}	2.05×10^{-1}	1.74×10^{-1}	1.74×10^{-1}
1.55	0.98	1	1.18×10^{-1}	1.29×10^{-1}	3.54×10^{-1}	-3.82×10^{-3}	1.16×10^{-1}	1.09×10^{-1}
1.55	0.98	3	2.09×10^{-1}	4.44×10^{-1}	1.60×10^{-1}	1.24×10^{-1}	1.08×10^{-1}	1.08×10^{-1}

leading to a time-independent and wave-packet-independent result. To demonstrate this, we choose wave packet No. 4 with an energy spread $\Delta E \approx 18$ MeV and the same initial polarization as above. This is sharp enough to produce a series of pictures, Fig. 6, which except at the very beginning are stationary.

It may be interesting to see the effect of individual meson exchanges on spin observables. As an example, Fig. 7 shows the polarization caused by pure pion exchange. Although there is some similarity to the full OBE dynamics shown in Fig. 3 quantitatively the time development and of course the final result are different.

VI. SUMMARY

Considering NN-scattering time dependently, allows us to see how momentum distributions for two nucleons change during the reaction time until they settle for large times to a distribution determined by the on-shell T matrix; it allows us to see for instance how from an initially unpolarized state the polarization of a nucleon builds up in time for each energy and scattering angle until it reaches the final measurable angular and energy dependent value. The initial wave packet contains a certain range of energies for which the calculation yields all observables in one shot. Some wave packets we use have an energy spread of 100 MeV or more and are centered around 50 or 100 MeV. Their extension in space is about 7 fm and the reaction time is about 200 fm or 7×10^{-22} sec. They are far away from the used realistic ones but useful for determining the observables for many energies in one run. The variation of the observables at intermediate times results from an interplay of the half-shell T matrix and the shape of the wave packet. For a wave packet centered at 50 MeV and having an energy spread of ≈ 18 MeV the spin observables turned out to be essentially stationary during the reaction time of about 1200 fm or 4×10^{-21} sec. Usual realistic wave packets are very much sharper in energy (of the order of 1 eV or below[8]) and a calculation of the time-dependent pattern of spin observables would yield perfectly stationary pictures over the very-long reaction time.

Studying the time-dependent process can also be used to determine bound states and binding energies. As an example we have chosen a wave packet located in the middle of the potential at $t=0$. In this manner the time-dependent state contains an appreciable admixture of the bound state which can be extracted for large times due to its specific frequency.

The NN potential we use is the OBE parametrization (OBEPR) of the new Bonn potential.[5] We use a momentum-space representation and work directly with vector variables avoiding partial-wave decompositions. Certainly for higher energies this appears advantageous. The time-dependent Schrödinger equation is rewritten into an integral equation which has the initial wave packet as the driving term. The time oscillations, $e^{-iE_q t}$, in momentum space seem to be at first glance very hard to control numerically in an integral equation for large times. We avoided that problem by choosing complex momenta, which leads to a rather smooth wave function and which goes to zero for large t values (besides near $q=0$). The wave function for real momenta can then be determined by quadrature and the on-shell t matrix can be extracted at large times. It was decisive in our algorithm to split the total reaction time into small intervals, within which we could interpolate the wave function in the time variable and perform the time integration analytically. The kernel propagating the wave function from one end to the other turned out to be independent of the respective interval. This was the key point in our algorithm for not unduly increasing the dimension of the problem due to the additional time variable.

The algorithm turned out to be very accurate, as documented for instance in the phase shifts calculated for the OBE potential. The complete absence of singularities induces us to think of applying the method to three-body systems. With increasing computer facilities this appears to be possible.

APPENDIX A

We consider ${}^{(+)}\langle \mathbf{q} \mid \psi_0(t_0)\rangle$ for $t_0 \to -\infty$. Introducing the t matrix we have

$$
\begin{aligned}
{}^{(+)}\langle \mathbf{q} \mid \psi_0(t_0)\rangle &= \langle \mathbf{q} \mid \psi_0(t_0)\rangle + \int d^3q' \frac{T^*(\mathbf{q}',\mathbf{q})}{E_q - i\epsilon - E_{q'}} \langle \mathbf{q}' \mid \psi_0(t_0)\rangle \\
&= e^{-iE_q t}\psi_0(\mathbf{q}) + \int d^3q' \frac{T^*(\mathbf{q}',\mathbf{q})}{E_q - i\epsilon - E_{q'}} e^{-iE_{q'}t_0}\psi_0(\mathbf{q}') \, . \qquad \text{(A1)}
\end{aligned}
$$

If one excludes an interval around the singularity at $E_q = E_{q'}$ the integral tends to zero because of the Riemann-Lebesgue lemma. In the remaining integral if the interval is chosen small enough we can remove $q'^2 T^*(\mathbf{q}',\mathbf{q})\psi_0(\mathbf{q}')$ from the integral and extend in the remaining one again the integration over all q'. Consequently

$$
\int d^3q' \frac{T^*(\mathbf{q}',\mathbf{q})}{E_q - i\epsilon - E_{q'}} e^{-iE_{q'}t_0}\psi_0(\mathbf{q}') \underset{t_0\to-\infty}{\to} \left[q^2 \int d\hat{\mathbf{q}}'\, T^*(\hat{\mathbf{q}}'q,\mathbf{q})\psi_0(\hat{\mathbf{q}}'q)\right] \int_0^\infty dq' \frac{1}{E_q - i\epsilon - E_{q'}} e^{-iE_{q'}t_0} \, . \qquad \text{(A2)}
$$

One can now deform the path of integration to $q' = \tau e^{i\pi/4}$, $\tau > 0$. Then the denominator becomes regular and the exponential function real and decreasing for $t_0 < 0$. In the limit $t_0 \to -\infty$ the integral behaves as $O(\mid t_0 \mid^{-1/2})$ as is easily estimated. As a result, only the first term in (A1) survives.

APPENDIX B

The OBEPR of the new Bonn potential[5] is reproduced. It is a sum of the following terms referring to pseudoscalar particles (π,η), scalar particles (σ,δ), and vector particles (ω,ρ):

$$\mathbf{V}^{(\mathrm{ps})}(\mathbf{q},\mathbf{q}')=-\left[\frac{1}{2\pi}\right]^3\frac{g_\beta^2}{4m^2}\frac{(\boldsymbol{\sigma}_1\cdot\mathbf{k})(\boldsymbol{\sigma}_2\cdot\mathbf{k})}{k^2+m_\beta^2}F_\beta^2(k^2)\ , \tag{B1}$$

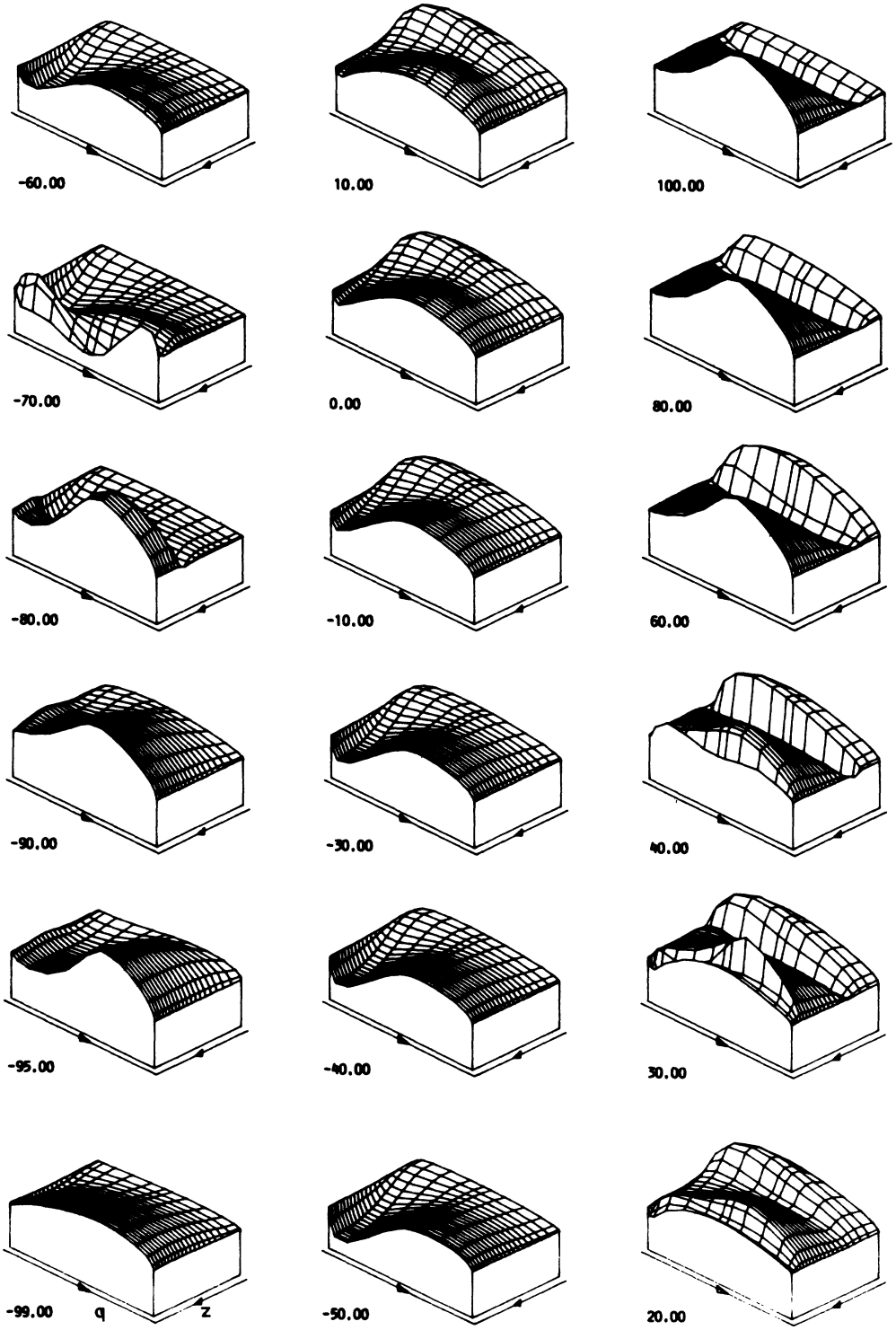

FIG. 7. The y component of $\mathbf{P}_0$ as a function of $z=\hat{\mathbf{q}}\cdot\hat{\mathbf{q}}_0$ and $q=|\mathbf{q}|$ for various times. This is for a pure one-pion-exchange interaction and wave packet No. 1. P_0 varies between -0.62 and 0.77.

TABLE VI. The parameters of the OBEPR (Ref. 5).

Mesons	I	S^P	m_β (MeV)	$g_p^2/4\pi$	f_β/g_β	Λ_β (GeV)
π	1	0^-	138.03	14.9		1.3
η	0	0^-	548.8	3		1.5
δ	1	0^+	983	2.6713		2.0
σ $(T=1)$	0	0^+	550	7.7823		2.0
σ $(T=0)$	0	0^+	715	16.2061		2.0
ρ	1	1^-	769	0.95	6.1	1.3
ω	0	1^-	782.6	20	0.0	1.5

$$\mathbf{V}^{(S)}(\mathbf{q},\mathbf{q}')=-\left[\frac{1}{2\pi}\right]^3\frac{g_\beta^2}{k^2+m_\beta^2}\left[1-\frac{\mathbf{p}^2}{2m^2}+\frac{k^2}{8m^2}-\frac{1}{4m^2}i(\boldsymbol{\sigma}_1+\boldsymbol{\sigma}_2)\cdot\mathbf{n}\right]F_\beta^2(k^2)\ , \tag{B2}$$

$$\begin{aligned}\mathbf{V}^{(V)}(\mathbf{q},\mathbf{q}')=\left[\frac{1}{2\pi}\right]^3\frac{1}{k^2+m_\beta^2}\Bigg[&g_\beta^2\left[1+\frac{3}{2}\frac{p^2}{m^2}-\frac{k^2}{8m^2}+\frac{3}{4m^2}i(\boldsymbol{\sigma}_1+\boldsymbol{\sigma}_2)\cdot\mathbf{n}-(\boldsymbol{\sigma}_1\cdot\boldsymbol{\sigma}_2)\frac{k^2}{4m^2}+\frac{1}{4m^2}(\boldsymbol{\sigma}_1\cdot\mathbf{k})(\boldsymbol{\sigma}_2\cdot\mathbf{k})\right]\\&+\frac{g_\beta f_\beta}{2m^2}[-k^2+2i(\boldsymbol{\sigma}_1+\boldsymbol{\sigma}_2)\cdot\mathbf{n}-k^2(\boldsymbol{\sigma}_1\cdot\boldsymbol{\sigma}_2)+(\boldsymbol{\sigma}_1\cdot\mathbf{k})(\boldsymbol{\sigma}_2\cdot\mathbf{k})]\\&+\frac{f_\beta^2}{4m^2}[-k^2(\boldsymbol{\sigma}_1\cdot\boldsymbol{\sigma}_2)+(\boldsymbol{\sigma}_1\cdot\mathbf{k})(\boldsymbol{\sigma}_2\cdot\mathbf{k})]\Bigg]F_\beta^2(k^2)\ .\end{aligned} \tag{B3}$$

The form factors are chosen in the form

$$F_\beta(k^2)=(\Lambda_\beta^2-m_\beta^2)/(\Lambda_\beta^2+\mathbf{k}^2)\ .$$

In the case of isovector particles, the terms are to be multiplied by $\boldsymbol{\tau}_1\cdot\boldsymbol{\tau}_2$. The parameters of OBEPR are given in Table VI.

APPENDIX C

With the abbreviations

$$u=qz,\quad u'=q'z',\quad \omega=q\sqrt{1-z^2},\quad \omega'=q'\sqrt{1-z'^2}\ , \tag{C1}$$

the explicit forms of the three types of 4×4 matrices occurring in the OBEPR of Appendix B are

$$i(\boldsymbol{\sigma}_1+\boldsymbol{\sigma}_2)\cdot\mathbf{n}=\begin{bmatrix}2i\omega\omega'\sin\varphi' & u\omega'e^{-i\varphi'}-u'\omega & u\omega'e^{-i\varphi'}-u'\omega & 0\\ -u\omega'e^{i\varphi'}+u'\omega & 0 & 0 & u\omega'e^{-i\varphi'}-u'\omega\\ -u\omega'e^{i\varphi'}+u'\omega & 0 & 0 & u\omega'e^{-i\varphi'}-u'\omega\\ 0 & -u\omega'e^{i\varphi'}+u'\omega & -u\omega'e^{i\varphi'}+u'\omega & -2i\omega\omega'\sin\varphi'\end{bmatrix}, \tag{C2}$$

$$(\boldsymbol{\sigma}_1\cdot\mathbf{k})(\boldsymbol{\sigma}_2\cdot\mathbf{k})=\begin{bmatrix}(u-u')^2 & (u-u')(\omega-\omega'e^{-i\varphi'}) & (u-u')(\omega-\omega'e^{-i\varphi'}) & (\omega-\omega'e^{-i\varphi'})^2\\ (u-u')(\omega-\omega'e^{i\varphi'}) & -(u-u')^2 & \omega^2-2\omega\omega'\cos\varphi'+\omega'^2 & -(u-\omega')(\omega-\omega'e^{-i\varphi'})\\ (u-u')(\omega-\omega'e^{i\varphi'}) & \omega^2-2\omega\omega'\cos\varphi'+\omega'^2 & -(u-u')^2 & -(u-u')(\omega-\omega'e^{-i\varphi'})\\ (\omega-\omega'e^{i\varphi'})^2 & -(u-u')(\omega-\omega'e^{i\varphi'}) & -(u-u')(\omega-\omega'e^{i\varphi'}) & (u-u')^2\end{bmatrix}, \tag{C3}$$

$$\boldsymbol{\sigma}_1\cdot\boldsymbol{\sigma}_2=\begin{bmatrix}1&0&0&0\\0&-1&2&0\\0&2&-1&0\\0&0&0&1\end{bmatrix}. \tag{C4}$$

The linear combinations $J_i^{(\alpha)}$ in (3.14) are

$$J_1^{(0)}=S_1,\quad J_2^{(0)}=\cos\varphi' S_2,\quad J_3^{(0)}=\cos2\varphi' S_3,\quad J_4^{(0)}=\cos\varphi' S_4,\quad J_5^{(0)}=S_5,\quad J_6^{(0)}=S_6\ ; \tag{C5}$$

$$\begin{aligned}&J_1^{(1)}=2(u\omega'-u'\omega\cos\varphi')S_2,\quad J_2^{(1)}=(-u\omega'\cos\varphi'+u'\omega)S_1+(u\omega'\cos\varphi'-\cos2\varphi' u'\omega)S_3\ ,\\&J_3^{(1)}=-2(u\omega'\cos2\varphi'-u'\omega\cos\varphi')S_2+4\omega\omega'\cos\varphi'\sin^2\!\varphi' S_3\ ,\end{aligned} \tag{C6}$$

$$
\begin{aligned}
&J_4^{(1)}=2\omega\omega'\sin^2\varphi' S_4+(u\omega'\cos\varphi'-u'\omega)(S_5+S_6)\ ,\\
&J_5^{(1)}=-2(u\omega'-u'\omega\cos\varphi')S_4,\quad J_6^{(1)}=J_5^{(1)}\ ;\\
&J_1^{(2)}=(u-u')^2S_1+2(u-u')(\omega\cos\varphi'-\omega')S_2+(\omega^2\cos2\varphi'-2\omega\omega'\cos\varphi'+\omega'^2)S_3\ ,\\
&J_2^{(2)}=(u-u')(\omega-\omega'\cos\varphi')S_1-[((u-u')^2-\omega^2-\omega'^2)\cos\varphi'+2\omega\omega'\cos^2\varphi']S_2-(u-u')(\omega\cos2\varphi'-\omega'\cos\varphi')S_3\ ,\\
&J_3^{(2)}=(\omega^2-2\omega\omega'\cos\varphi'+\cos2\varphi'\omega'^2)S_1+2(u-u')(-\omega\cos\varphi'+\omega'\cos2\varphi')S_2+(u-u')^2\cos2\varphi' S_3\ ,\\
&J_4^{(2)}=\{[(u-u')^2-\omega^2-\omega'^2]\cos\varphi'+2\omega\omega'\}S_4+(u-u')(\omega-\omega'\cos\varphi')(S_5+S_6)\ ,\\
&J_5^{(2)}=2(u-u')(\omega\cos\varphi'-\omega')S_4-(u-u')^2S_5+(\omega^2-2\omega\omega'\cos\varphi'+\omega'^2)S_6\ ,\\
&J_6^{(2)}=2(u-u')(\omega\cos\varphi'-\omega')S_4+(\omega^2-2\omega\omega'\cos\varphi'+\omega'^2)S_5-(u-u')^2S_6\ ;
\end{aligned}
\tag{C7}
$$

$$
\begin{aligned}
&J_1^{(6)}=S_1,\quad J_2^{(6)}=\cos\varphi' S_2\ ,\\
&J_3^{(6)}=\cos2\varphi' S_3,\quad J_4^{(6)}=\cos\varphi' S_4\ ,\\
&J_5^{(6)}=-S_5+2S_6,\quad J_6^{(6)}=2S_5-S_6\ .
\end{aligned}
\tag{C8}
$$

In the OBEPR the terms V_α, $\alpha=3,4,5$, do not occur separately and are set to zero. There occurs instead the term $\sigma_1\cdot\sigma_2$ to which we associate a term V_6 and correspondly the $J_\alpha^{(6)}$ above.

[1]Y. Sun, R. C. Mowrey, and D. J. Kouri, J. Chem. Phys. **87**, 339 (1987), and references therein.

[2]A. Goldberg, H. M. Schey, and J. L. Schwartz, Am. J. Phys. **35**, 177 (1967).

[3]J. Holz and W. Gloeckle, J. Comput. Phys. (to be published); in *Proceedings of the International Workshop on Few-Body Approaches on Nuclear Reactions in Tandem and Cyclotron Energy Regions,* edited by S. Oryu and T. Sawada (World Scientific, Singapore, 1987), p. 3.

[4]J. Holz, Ph.D. thesis, University of Bochum, 1987.

[5]R. Machleidt, K. Holinde, and Ch. Elster, Phys. Rep. **149**, 1 (1987).

[6]L. Wolfenstein and J. Ashkin, Phys. Rev. **85**, 947 (1952).

[7]T. Hippchen (private communication).

[8]N. Austern, *Direct Nuclear Reaction Theories* (Wiley, New York, 1970).